

A novel application of cryogenics in dieless sheet metal piercing

Paolo Albertelli^{1,a*}, Valerio Mussi^{2,b} and Michele Monno^{1,a}

¹Mechanical Engineering Department, Politecnico di Milano, via la Masa 1, 20156 Milan, Italy

²Consorzio MUSP via Callegari, 29122 Piacenza, Italy

^apaolo.albertelli@polimi.it, ^bvalerio.mussi@musp.net, ^cmonno.michele@polimi.it

Keywords: Piercing, Cryogenic, Constitutive Models

Abstract. In tube punching, if the internal die is necessary to properly pierce the tube avoiding its collapse, it also represents a bottleneck to a rapid change of the punching set. In this research an innovative dieless tube punching approach has been conceived and studied. The use of a cryogenic fluid to force the material ductile-brittle transition is a way to limit the sheet deformation during the piercing process. The analysis of the innovative cryogenic punching was carried out both adopting numerical and experimental methodologies. A finite element FE model of the cryogenic punching was developed and updated in two stages. First, experimental tensile tests, performed at cryogenic temperatures, were used to characterize some material properties. Secondly, some piercing tests in cryogenic conditions were performed at different velocities and temperatures to fine update the model. A validation session was carried out to assess the model and the process feasibility. It was found that the FE model reproduced the experimental results within a maximum estimation error of 10% on both the punching force and tube deflection. Results showed that both the increment of the punching velocity and especially the decrement of the punching temperature could be the only viable solution for making the tube dieless punching industrially feasible.

Introduction

The use of cryogenic fluids in manufacturing processes represents a rather new research branch. Jawahir et al. in [1] critically reviewed the main applications in which cryogenics are used in manufacturing and they outlined the most relevant opportunities and challenges in the field. Some aluminum alloys show a high deformability at cryogenic temperatures [2] that is used in several processes like deep drawing or extrusion to produce more complex parts. Conversely, although the ductile-brittle transition of some materials (e.g., body-centered cube bcc materials) at low temperatures is well known, this material feature has not yet been exploited in manufacturing processes. To bridge this gap, in this study it has been investigated the possibility to exploit the ductile-brittle transition that occurs at cryogenic temperatures for making the dieless punching feasible from the product quality perspective. The novelty of this research is associated to the development of a cryogenic punching model that can be used to robustly estimate the required punching force and the tube deformation according to the specific adopted process parameters. The paper is structured as follows. In the material and methods section, a first process description was provided. The modelling aspects, both considering the FE modelling and the material rheological behavior were reported. The strategy to update the model and the design of experiments were also presented. The results and discussion section presents the main experimental findings and a proper validation of the conceived modelling approach.

Materials and Methods

In this paper section, a description of the innovative dieless cryogenic tube piercing process was provided. A conceptual comparison between the regular tube punching process and the cryogenic dieless punching was reported in Fig. 1 a) and b). Since some materials show a ductile-brittle transition at cryogenic temperatures, the possibility to pierce a tube without the internal die but, at

the same time, limiting the sheet deformation has been investigated, Fig. 1 c) and d). The first implementation of the cryogenic punching process was depicted in Fig. 1 e). It is worth of noting that the tube is cooled by an inner flow on liquid nitrogen LN. The tube is hold by the bottom part of the external die while the punch and the upper part of the die can move vertically to allow the tube feed after the piercing execution. In this specific cryogenic punching release, a 30mmx30mm tube of S235JR steel with a thickness of 2.45mm was adopted. The punch diameter is equal to 10mm. Additional information on the experimental set-up were provided in the Design of Experimental session. In the following subsections details regarding the model development, calibration and validation are provided.

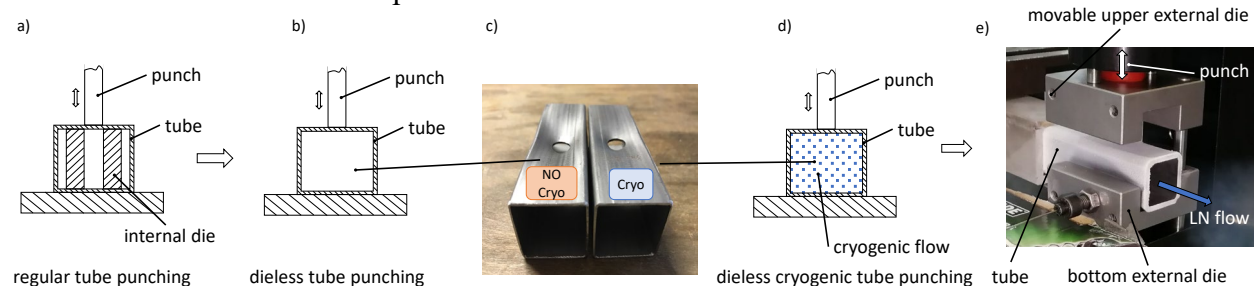


Fig. 1: a) regular tube punching b) dieless tube punching c) tube deformation in dieless punching (cryogenic vs no cryogenic) d) cryogenic punching e) cryogenic experimental set up.

Finite Element modelling

The FE model was developed in with ForgeNxT2.1. Three-dimensional finite elements (tetrahedrons with five nodes and linear interpolation) were used for meshing the punch and the tube. The implemented formulation allows considering both the deformation mechanics and thermal equations. An implicit integration scheme, with the Newton-Raphson method was used. An overview of the dieless punching process model, its main settings, the main approach adopted for its updating and validation are reported in Fig. 2 a) e c). Additional details will be provided in the model updating section. Four mesh regions were defined. The mesh size was refined in three specific regions as reported in Fig. 2 b). It was decided to model the punch as a rigid body since the deformation is mostly related to the tube. Even the tube supports (external equipment) were modelled as rigid bodies.

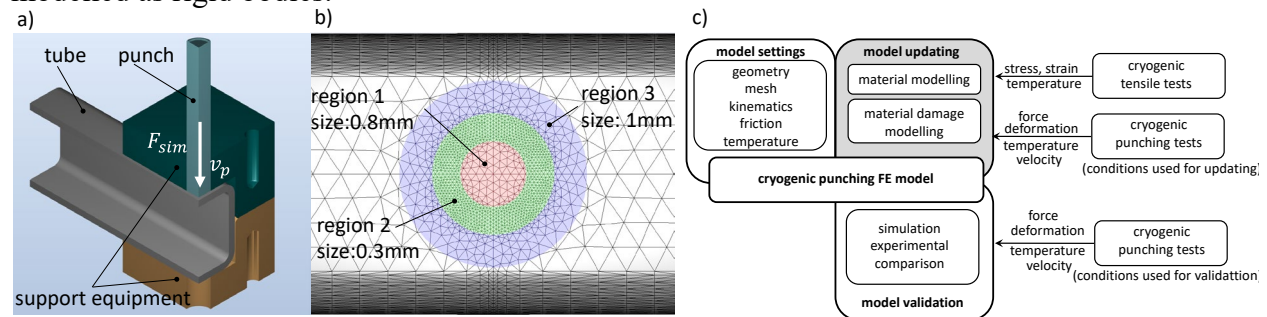


Fig. 2: a) Dieless tube punching modeling b) mesh regions c) model settings and updating.

In accordance with the experimental set-up, the punch stroke was set equal to 8mm. The punch velocity v_p was considered constant during the punching. The range of 4-140mm/s for the punching velocity was considered for the simulations. An upper threshold for the punching force F_{sim} was imposed to reproduce the pressure limitations associated to the hydraulic units used for driving the punch, see the Design of Experiments session. Indeed, if the resulting punching force overcomes the threshold the simulation is quitted. Regarding the punching temperature T_p , according to the described implementation of the cryogenic process (Fig. 1), it was set uniformly into the whole tube while the punch temperature was set equal to the environmental temperature (20°C). The heat exchange between the tube and the punch/environment was limited since a steady

state punching temperature was assured by a calibrated flow of liquid nitrogen inside the tube. For what concerns the punch-tube contact, the chosen friction model was a stick-slip Coulomb-Tresca model (Eq. 1). μ is the friction coefficient, m_f the friction factor, τ the shear stress, σ_n the normal pressure and τ_{lim} the yield shear stress which depends on the material flow stress σ according to Von-Mises.

$$\begin{aligned} \tau &= \mu \cdot \sigma_n && \text{when } \mu \cdot \sigma_n < m_f \cdot \tau_{lim} \\ \tau &= m_f \cdot \tau_{lim} && \text{when } \mu \cdot \sigma_n \geq m_f \cdot \tau_{lim} \end{aligned} \quad (1)$$

In the developed model, the following values were adopted $\mu = 0.4$; $m_f = 0.8$.

Material modelling

It was decided to adopt the basic Johnson-Cook (JC) formulation [3], described as follows $\sigma = (A + B\varepsilon^n)(a + C \cdot \ln(\dot{\varepsilon}/\varepsilon_0))(1 - ((T - T_0)/T_m - T_0)^m)$. σ is the flow stress, $\dot{\varepsilon}$ the strain rate, T_m and T_0 are respectively the melting temperature and a reference temperature. A is the initial yield stress, B allows considering the material hardening phenomenon, n is the index associated to the strain sensitivity, C is the index that considers the dependency due to the strain rate, ε_0 is the reference value for the strain rate and m is the coefficient that considers the temperature dependency. The innovative aspect of the present study is related to the characterization of the material behavior at the cryogenic temperatures. Thus, a strategy for the model parameter identification was conceived. For what concerns the damage modelling, it was decided to adopt the Latham-Cockcroft LC formulation $D = \int_0^{\varepsilon_f} \sigma_I d\varepsilon$ that is the most established approach for modelling fracture after large strain deformation. D is the threshold value that is used for eliminating the damaged elements during the simulations, σ_I is the highest principal component of the stress tensor, and ε_f is the limit fracture strain. More specifically, the critical damage value is calculated for each element under deformation at each time-step. Once the damage value in an element reaches the critical one, a crack is initiated in two steps: (i) this element is deleted with all the parameters related to it, including element connectivity definition, the strain and stress values; (ii) the rough boundary produced by element deletion is smoothed by cutting out the considered rough angle and adding new points.

Model Simulations and settings

The developed model was used to simulate the dieless punching process. Specifically, the tube deformation d_t (including the maximum value $d_{t,max,sim}$, the stress and the strain distribution and the punching force F_{sim} (including its maximum value $F_{sim,max}$) can be estimated. For sake of example, some simulation outputs were shown in Fig. 3 a) and b) and c).

Model Updating Strategy

The model updating procedure is summarized in Fig. 3 d). For what concerns the Johnson-Cook model parameters, the following strategy was adopted. A, B, n were identified from quasi-static test (tensile tests) at the reference temperature (-80°C). The tensile tests were executed considering a reference strain rate ($\dot{\varepsilon}_0 = 0.002/s$) to neglect the strain rate effect. The adopted conditions also allow neglecting the temperature related term. Three specimens were used, and the average nominal stress-strain curve was computed for the identification process. The approach suggested in Schwab and Harter [4] was adopted to estimate the true stress strain curve $\sigma = f(\varepsilon)$ from the corresponding nominal quantities (s and e). The identification of the parameters was twofold. First, the A parameter was identified as the initial yielding stress.

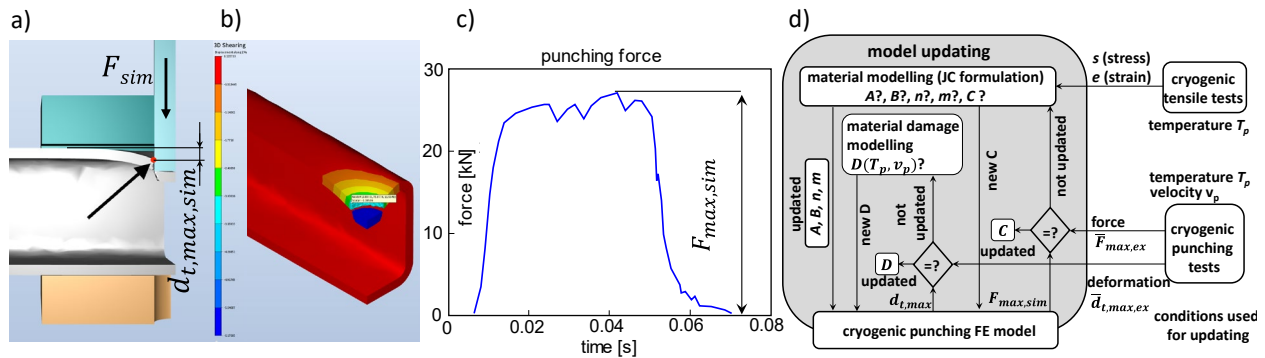


Fig. 3: Example of FE model simulations a) maximum tube deflection estimation $d_{t,max,sim}$ b) deformation map c) punching force $F_{max,sim}$ d) model updating procedure

In the second step, a regression procedure performed on the tensile test data corresponding to the homogeneous plastic deformation region, thus excluding both the elastic and necking region, was carried out for the identification of B and n. m is calculated using the results of tests (tensile tests) at different temperatures. (-80°C , -60°C , -40°C). For each temperature T , the stress σ data associated to different strain values ($\varepsilon_1 = 0.1$, $\varepsilon_2 = 0.15$, $\varepsilon_3 = 0.2$) were used. Starting from the JC formulation and introducing $K = (A + B\varepsilon^n)$, the following relationships can be obtained $\ln(1 - \sigma/K) = m \cdot \ln((T - T_0)/(T_m - T_0))$. As a result, the identification of the m parameter was done through a linear regression of the experimental data. See Results and discussion session session, Table 3. C is updated comparing the results (simulations and experimental data) of the punching tests in terms of cutting forces (F_{max}). In Fig. 3 c) an example of the simulated piercing force was reported. This approach was used to characterize the contribution of the strain rate in realistic conditions that are not achievable through tensile tests since the feed velocity of the tensile machine crossbar is generally rather limited. Additional details on the experimental force measurements were provided in the next paper session. Regarding the LC model parameter D, in this work, it was decided to characterize the material damaging considering the combined effect of temperature and strain rate. To accomplish it, a procedure based on experimental punching tests performed at different punching temperatures T_p and different punching velocities v_p was adopted. As a result, the formulation of the LC model can be resumed as $D = D(v_p, T_p)$. According to what reported in Fig. 3 d), for each tested condition, the FE model was updated, properly tuning the D parameter, to get the experimental maximum tube deflection $d_{t,max}$. Additional details on experimental measurement of the tube deflection were provided in the next session.

Design of Experiments and equipment description

Tensile tests

As previously described in the Model Updating Strategy, the tensile tests were carried out at five T_t temperatures (-80°C , -60°C , -40°C , 0°C and 20°C). For each temperature, three specimens were tested. According to ISO 6892-3 [5], a flat tensile test specimen with shoulders was used, Fig. 4 c). The specimen was characterized by a nominal cross-sectional area (6mm (width) x 2.45mm (thickness)) and a calibrated length equal to 25mm. The specimens were manufactured through abrasive water jet technology starting from the same tube batch. In order to take into account the process accuracy and variability, the cross-sectional dimensions of each single specimen were measured. The MTS Alliance RF/150 tensile test machine, equipped with the MTS 651-environmental chamber, was used, Fig. 4. The machine has a thermal room able to reach different temperatures. In these tests the room was fed by nitrogen until the defined temperature is reached. The specimens to be tested at this temperature were positioned inside the chamber to reach the thermal equilibrium.

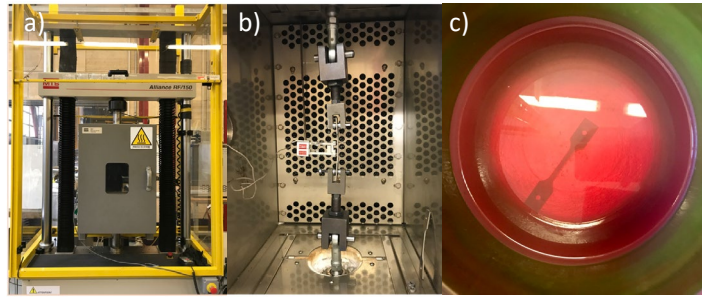


Fig. 4: a) Tensile test machine b) tensile test c) cryogenic chamber and specimen

The velocity of the crosshead that holds the specimens was equal to 4 mm/min , that corresponds to $\dot{\epsilon}_0$. During the tensile tests, the crosshead position, the extensometer data (specimen extension) and the applied load were acquired with a time span of 0.1s. The data were used to compute the nominal stress and strain.

Punching tests

According to the model updating approach conceived for the identification of both the C parameter (JC) and the damage material behaviour $D = D(v_p, T_p)$, it was necessary to perform piercing tests in different conditions both in terms of temperatures and punching velocities. For this purpose, a 2-level factorial approach with a center point (intermediate conditions) was adopted. For each punching conditions three repetitions were executed. The punching tests were executed in randomized order. Table 1 resumes the tested conditions. The conditions used for updating the model and the ones used for the model validation were indicated, last column of Table 1.

Table 1: design of experiments – punching tests

Test condition ID	hydraulic unit HU	punching velocity v_p [mm/s]	punching temperature T_p [°C]	updating parameter (measured quantity)
ID1	HU1	$v_{p,high}$	$T_{p,high}$	updating $D(d_{t,max,ex})$, $C(F_{max,ex})$
ID2	HU1	$v_{p,high}$	$T_{p,mid}$	updating $C(F_{max,ex})$
ID3	HU1	$v_{p,high}$	$T_{p,low}$	updating $D(d_{t,max,ex})$
ID4	HU2	$v_{p,mid}$	$T_{p,high}$	validation
ID5	HU2	$v_{p,mid}$	$T_{p,mid}$	updating $D(d_{t,max,ex})$
ID6	HU2	$v_{p,mid}$	$T_{p,low}$	validation
ID7	HU3	$v_{p,low}$	$T_{p,high}$	updating $D(d_{t,max,ex})$
ID8	HU3	$v_{p,low}$	$T_{p,mid}$	validation
ID9	HU3	$v_{p,low}$	$T_{p,low}$	updating $D(d_{t,max,ex})$

More specifically, in accordance with the explanation provided in the previous session and schematized in Fig. 3 d), Table 1 describes the experimental data, reported in brackets, used for tuning the specific model parameter. The FE model parameters tuning was considered achieved when the experimental/simulated matching was limited to a percentage error of about 3%. The punching tests were carried out with the equipment described in Fig. 5. The actuator cylinder Fig. 5 a) and b) directly drives the punch through the pressurized oil provided by the hydraulic unit HU Fig. 5 a). The punching temperature was set making the LN flows inside the tube, see Fig. 1 b) and Fig. 5 c). The LN flow rate was tuned, through the regulating valve, to set the desired tube temperature T_p . A thermocouple (see Fig. 5 c)) was used to monitor the temperature. Three temperature levels were considered $T_{p,low} = -80^\circ\text{C}$, $T_{p,mid} = -40^\circ\text{C}$ and $T_{p,high} = 20^\circ\text{C}$. To change the punching velocity v_p , three different hydraulic units were used, see Table 1. Since no detailed information about the hydraulic units were available, an experimental characterization

was carried out. Several air punching tests (without the tube) were executed to measure the average punching velocity. This was done exploiting an eddy current sensor that was installed to detect the punch motion.

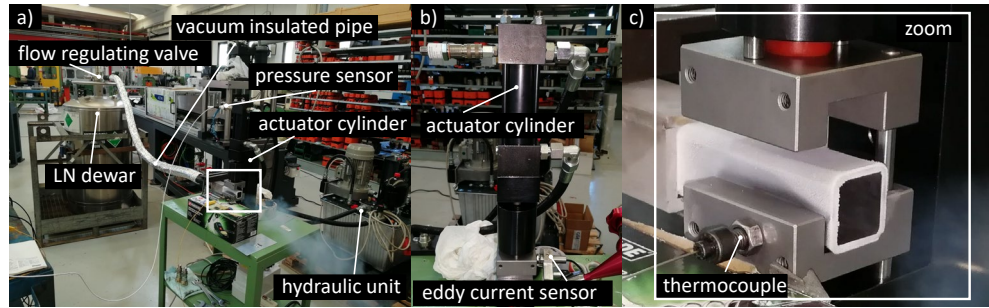


Fig. 5: a) experimental set up and sensors, b) actuator cylinder, c) process details and thermocouple for temperature measurements

From this experimental characterization it was found that respectively HU1 allowed to set a nominal punching velocity $v_{p,high} = 731.4mm/s$, HU2 a punching velocity of $v_{p,mid} = 156.6mm/s$ and the HU3 a punching velocity of $v_{p,low} = 44.5mm/s$. Since each hydraulic unit has its own control unit and its dynamic properties, the real average punching velocities were also computed exploiting the experimental piercing data. It is worth of noting that the calculated real velocities and the maximum achievable pressures were properly set in the simulation FE model. As previously described, both for model updating and for validation, the maximum punching force F_{max} and the maximum tube deflection $d_{t,max}$ were exploited. The punching force $F_{max,ex}$ was estimated measuring the cylinder inner pressure (pressure sensor, Fig. 5 a) and knowing the cylinder area that is equal to $1256mm^2$. The tube deflection was measured scanning the upper tube area with Alicona infinite focus. For each tube, the $d_{t,max,ex}$ were measured. Since three repetitions were carried out for each piercing condition, the average values were computed ($\bar{d}_{t,max,ex}, \bar{F}_{max,ex}$).

Results and discussion

In this section the main results in terms of material modelling development and cryogenic punching modelling were reported. As described in the Model updating strategy section, most of the JC parameters (A, B, n, m) were identified from the tensile test data. All the identified parameters were reported in Table 2. Fig. 6 a) shows the results of experimental tensile tests performed at different temperatures while Fig. 6 b) shows the effect of the temperature on the identified JC model. Regarding the Lathan Cockcroft model, the following formulation (Eq. 2) was developed through a regression procedure that shows a $R^2 = 0.98$ and an adjusted value of $R_{adj}^2 = 0.91$.

$$D = D(v_p, T_p) = 0.831 - 0.000154 \cdot V_p + 0.003278 \cdot T_p + 2.761 \cdot 10^{-5} \cdot V_p \cdot T_p \quad (2)$$

Table 2: JC identified model parameters (reference temperature $-80^\circ C$)

A [MPa]	B [MPa]	n	C	m	$\epsilon_0 [s^{-1}]$
460	150	0.1	0.045	0.53	0.002

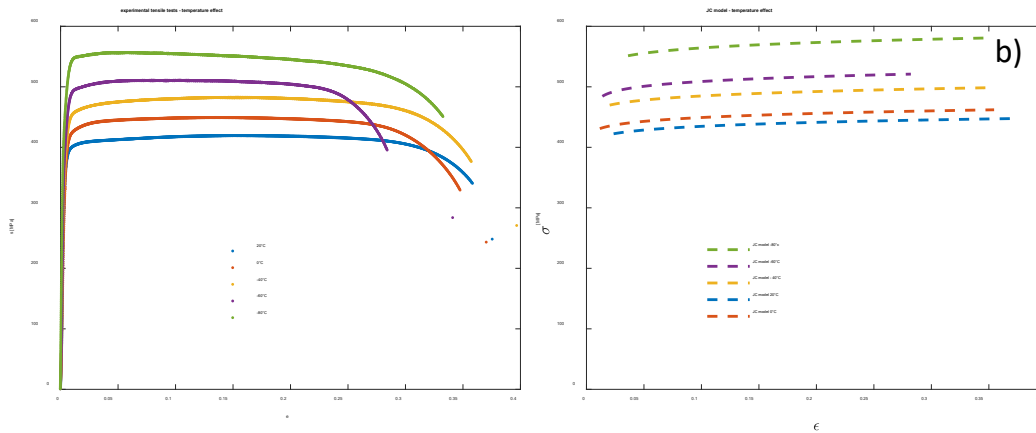


Fig. 6: effect of temperature: a) experimental tensile test data (average on three specimens) b) identified JC model and effect of temperature.

Both the formulations (refer to Table 2 and Eq. 2) were implemented in Forge to perform the punching simulations. As anticipated in Table 1, some of the test conditions were used to calibrate the model according to the experimentally measured tube deflection and punching force while some other test conditions were used to validate developed FE model. Among brackets were reported the updated numerical quantities. Table 3 resumes the main achieved results in the tested conditions. The percentage errors in both the maximum force $e_F = 100(F_{max,sim} - \bar{F}_{max,ex})/\bar{F}_{max,ex}$ and tube deflection estimation $e_d = 100(d_{t,max,sim} - \bar{d}_{t,max,ex})/\bar{d}_{t,max,ex}$ were reported. In addition, the real average punching velocities were also shown. As anticipated, they were computed for each HU and considering each specific punching conditions (ID). They were estimated analysing the experimental pressure profiles. It was found that the real punching velocities are much lower than the corresponding nominal ones (measured during air punching experiments) due to the dynamic behaviour of the HU and of its control unit under the effect of the punching load.

Table 3: Experimental results and validation of the model.

ID	HU	v_p [mm/s]	T_p [°C]	$\bar{F}_{max,ex}$ [kN]	$F_{max,sim}$ [kN]	$\bar{d}_{t,max,ex}$ [mm]	$d_{t,max,sim}$ [mm]	e_F [%]	e_d [%]
ID1	HU1	137	20	23	(23.2)	3.95	(3.82)	(0.9)	(-3.3)
ID2	HU1	105	-40	25.1	(25.1)	3.48	3.38	(0)	-2.9
ID3	HU1	85	-80	28.6	27.4	2.79	(2.74)	-4.2	(-1.8)
ID4	HU2	20	20	22.2	22.23	3.92	(3.79)	0.1	(-3.3)
ID5	HU2	10	-40	25.3	24.4	3.89	3.53	-3.6	-9.3
ID6	HU2	4.5	-80	28.3	25.43	3.53	(3.44)	-10.1	(-2.5)
ID7	HU3	20	20	22.5	22.23	3.9	(3.79)	-1.2	(-2.8)
ID8	HU3	20	-40	25.7	24.9	3.55	(3.49)	-3.1	(-1.7)
ID9	HU3	20	-80	28	26.3	3.16	3.24	-6.1	2.5

It can be observed that the model reproduces the experimental data with a maximum error of 10% both on the punching force and tube deflection. This demonstrates that the developed material models, suitable for describing its behaviour at cryogenic temperatures, and the FE model can be considered rather accurate and can be used for predicting the sheet deformation and the punching force involved in the process. The developed model can be rather useful to design a new dieless punching system especially in the definition of its specifications in term of maximum punching force, punching velocity and punching temperature to be adopted. Referring to the specific analyzed case, considerations on the effect of the punching velocity and temperature can be carried

out. Specifically, the temperature has a strong effect on both the punching force and on the maximum tube deflection. It was found that averagely the punching force increases of about 20% decreasing the T_p from 20°C to -80°C while the tube deflection decreases of about 29%. The effect of the punching velocity is limited with respect to the one associated to the temperature. This is more evident on the tube maximum deflection than on the punching force. Moreover, it seems that the punching velocity shows its effect mainly at cryogenic temperatures (-80°C). Indeed, in such conditions the deflection decreases of about 20% if the punching velocity is increased from 4.5mm/s to 85mm/s. At -40°C the tube deflection decreases of about 12% increasing the punching velocity from 10mm/s to 105mm/s while at 20°C the effect of the punching velocity seems negligible.

Conclusions

In this research, the use of cryogenics for dieless tube punching was explored. Both experimental cryogenic punching tests and numerical simulations of the process were carried out. Specifically, a FE model was developed and properly updated in terms of rheological material behavior. For this purpose, both punching tests, executed at different temperatures and velocities, and tensile tests carried out at different velocities were done. The experimental data (punching force and tube deformation) were exploited to identify the parameters of both the JC and LT models that feed the FE model. The estimating capabilities of the FE model were assessed considering some validation test conditions. The model showed quite good performances. Indeed, estimation errors lower than 10% on the maximum punching force and maximum tube deflection were observed. It was noted that the punching velocity seems affecting the tube deformation only at cryogenic temperatures. Although the execution of the dieless punching at cryogenic temperatures (-80°C) with the maximum achievable punching velocity (considering the equipment available in this research) allowed reducing the tube deformation, the result seems still much higher than the ones obtained with the regular tube punching process. According to the described results, to make the cryogenic punching a feasible solution for piercing the tubes without the internal die, it would be necessary to investigate the performance even setting lower punching temperatures and especially imposing a much higher velocity to the punch. For this purpose, a specific punching control unit should be developed. An electric drive seems more adequate for the implementation of this innovative process.

References

- [1] I.S. Jawahir, H. Attia, D. Biermann, J. Duflou, F. Klocke, D. Meyer, S.T.T. Newman, F. Pusavec, M. Putz, J. Rech, V. Schulze, D. Umbrello, Cryogenic manufacturing processes, *CIRP Ann Manuf Technol.* 65 (2016) 713–736. <https://doi.org/10.1016/j.cirp.2016.06.007>
- [2] X. Wang, X. Fan, X. Chen, S. Yuan, Forming limit of 6061 aluminum alloy tube at cryogenic temperatures, *J Mater Process Technol.* 306 (2022) 117649. <https://doi.org/10.1016/J.JMATPROTEC.2022.117649>
- [3] P. Albertelli, M. Strano, M. Monno, Simulation of the effects of cryogenic liquid nitrogen jets in Ti6Al4V milling, *J Manuf Process.* 85 (2023) 323–344. <https://doi.org/10.1016/J.JMAPRO.2022.11.053>
- [4] R. Schwab, A. Harter, Extracting true stresses and strains from nominal stresses and strains in tensile testing, *Strain.* 57 (2021). <https://doi.org/10.1111/STR.12396>
- [5] ISO 6892-3, *Metallic Materials - Tensile testing - part 3*, (2015).